Stereoscopic PIV Measurements of Transition in Pipe Flow, Measurement Uncertainty in Laminar and Turbulent Flow

by
C.W.H. van Doorne, J. Westerweel and F.T.M. Nieuwstadt

Laboratory of Aero- and Hydrodynamics, Delft University of Technology and
J.M. Burgerscentrum, The Netherlands.
E-mail: c.w.h.vandoorne@wbmt.tudelft.nl , j.Westerweel@wbmt.tudelft.nl ,
f.t.m.Nieuwstadt@wbmt.tudelft.nl.

Abstract

A stereoscopic PIV system was build to study laminar turbulent transition in pipe flow. The PIV system is based on an angular displacement of the two cameras and a 3D calibration based reconstruction method. In order to measure the cross flow over the entire cross section of the pipe, the light sheet is perpendicular to the main flow direction. Measurements have shown that the PIV system is capable of detecting the laminar and turbulent flow fields over a large portion of the pipe cross section (fig.1), with increasing errors in the near wall region.
In the error analysis, estimations and measurements of the registration error are shown (fig.2). The registration error is due to a small misalignment of the light sheet and the calibration plane. It is shown to make an important contribution to the total error. The transition measurements presented at the end of the paper are the result of brief test runs and are a good example of the kind of experiments planed for the near future.

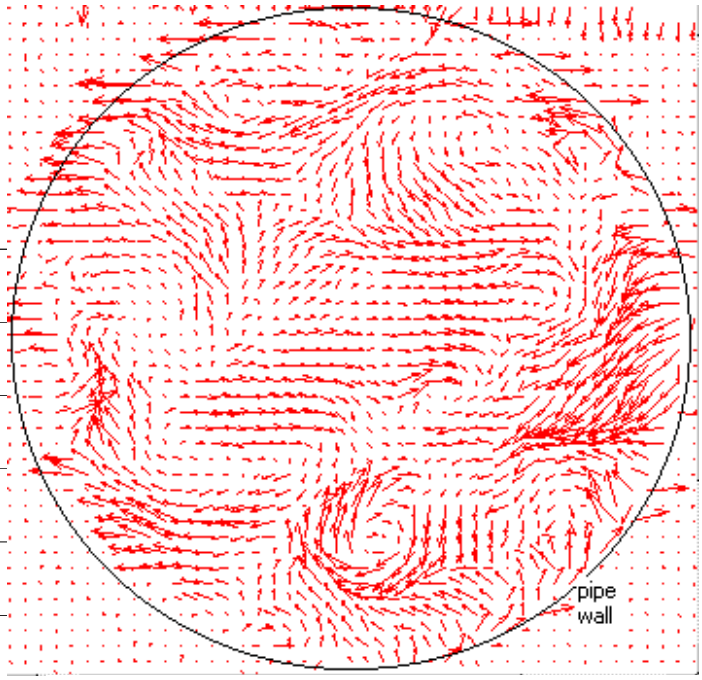

Fig.1. Piv measurement of turbulent pipe flow at Re=5300.

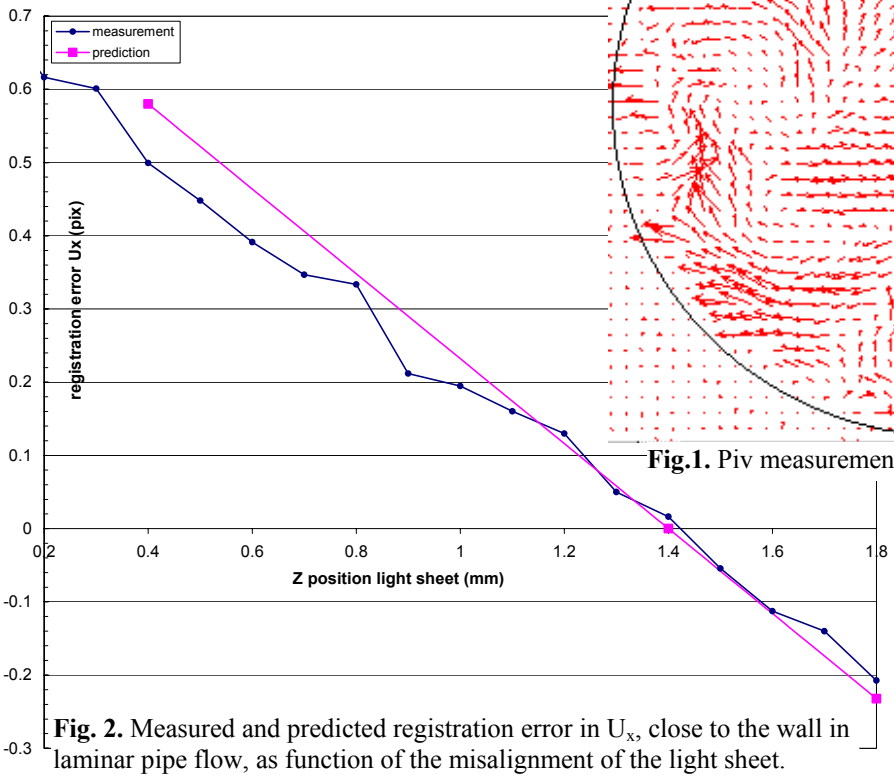

Fig. 2. Measured and predicted registration error in U_x, close to the wall in laminar pipe flow, as function of the misalignment of the light sheet.

1. Introduction

Laminar Turbulent transition in pipe flow was first studied in 1883 by Reynolds (1883). And despite this long history and many investigations, it is still not well understood. One of the difficulties is that the laminar parabolic velocity profile is linearly stable. This means that transition must start from a disturbance with finite.amplitude. The disturbance may have any form. For comparison of numerical and experimental work it is important that the initial flow disturbances are well defined and similar. A frequently used disturbance is periodic blowing and suction from the wall, see e.g. Ma *et al.*(1999) and Eliahou *et al.*(1998).

Our research is a continuation of the work by Draad *et al.(1998)* and Westerweel (1996) *et al*., who considered injection in pipe flow and reconstructed a turbulent slug by combining a sequence of PIV data fields. Our goal is to design a new disturbance mechanism that introduces laminar flow perturbations of which the results are comparable with numerical and theoretical work. The downstream evolution of the perturbation will be studied by using stereoscopic PIV. Compared to the previous experiments (Westerweel *et al.*(1996)) the orientation of the light sheet has changed and is now perpendicular to the pipe. The reason for such orientation of the light sheet is that we want to measure the streamwise vortices as they appear in the DNS simulations of Ma *et al.(1999).*

In this paper we will present the PIV set up used for our measurements and discuss the measurement uncertainty of the system. Special attention is paid to registration errors. Having a laminar shear flow at hand (Poiseuille flow), we are able to measure the registration error directly and verify our conceptual understanding of it. The transition measurements presented at the end of this paper are the result of brief test runs and show the validity of the measurement concept and are examples of the kind of experiments we will conduct in the near future.

2. Experimental setup and procedures

Figure 3 shows the layout of the experimental set up. The pipe flow facility is described in detail by Draad (1996). The pipe is 650 pipe diameters long, 40 mm in diameter and due to a well designed contraction and thermal isolation of the pipe, the flow can be kept laminar up to Re=60.000. The working fluid is water.

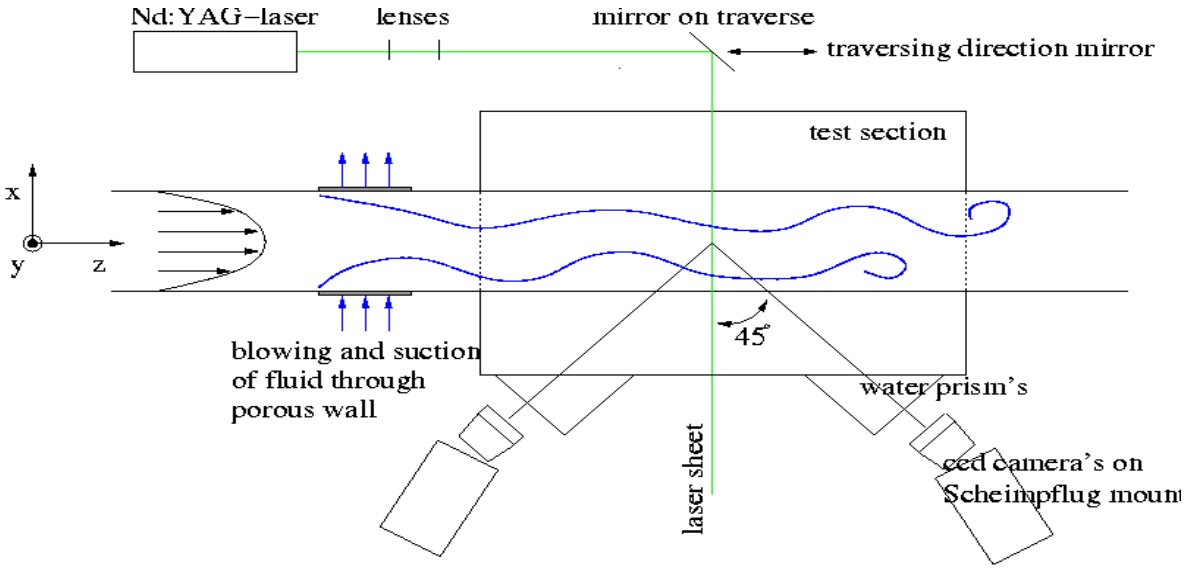

Fig. 3. Schematic of experimental setup.

The stereoscopic PIV system makes use of an angular displacement of the cameras and satisfies the Scheimpflug condition. A 3d calibration based reconstruction is used to evaluate the recordings. Both cameras look at an angle of 45° to the object plane. The two cameras are placed in the forward scattering direction of the laser light and therefore stand on different sides of the light sheet. This arrangement of the cameras was first used by Willert (1997). The cameras receive enough light from particles in the filtered tap water (a 10 micro-meter filter was used) so that there was no need to add extra particles.

The light sheet is perpendicular to the main-stream in order to measure streamwise vortices. This orientation of the light sheet results in large out of plane motion and limits the particle displacements to relatively small values (up to 10 pixels gives good correlation). This in turn leads to a significant decrease in the dynamic range of the system and the accuracy in the cross flow. Under optimal conditions we can resolve displacements of 0.1 pixel, which is 1% of the maximal displacement. In transitional flow, the velocity fluctuations are also of the order of a few percent of the bulk velocity and one might wonder if we will be able to resolve this.

The laser is a double pulsed Nd:YAG laser with a power of 200 mJ/pulse. The two Kodac ES 1.0 cross-correlation camera's operate at 15 Hz and give images of 1008x1008 pixels. To minimise optical distortion of the image, two water prisms are placed in front of the test section.

The reconstruction of the 3D vector field from the 2 displacement fields of camera 1 & 2 is based on a 3D calibration of the system as explained by Solov *et al.* (1997) and Prasad (2000). The calibration grid is recorded at several z-positions (instead of 1 for 2D calibrations) and the method does not require the input of any geometric parameter of the set up.

To place a calibration grid in the set up such that it can be seen from both sides by cameras 1 & 2 and over the full cross section of the pipe is not trivial. The calibration grid used so far is shown in figure 4. At first we used a 2 mm spaced lattice printed on overhead sheet. Due to heating the sheet becomes curved after printing in most printers, thus the choice of the printer is important. The grid is kept in position by a transparency sheet rolled-up in a cylinder, which in turn is held by a plastic rod, which precisely fits into the pipe. The cylindrical transparency sheet forms a solid support for the grid and leaves optical access to both sides of the grid without any noticeable optical distortion. We didn't find good glue for the overhead sheet, which also can withstand water. Therefore the sheet is fused together at some points by applying heat. To place the calibration grid in the pipe, a special water tank is placed after the test section (fig. 5). After calibration the tank must be removed and the system is closed again. The smallest change in position of the test section would make the calibration useless and therefore the test section is fixed firmly to a support.

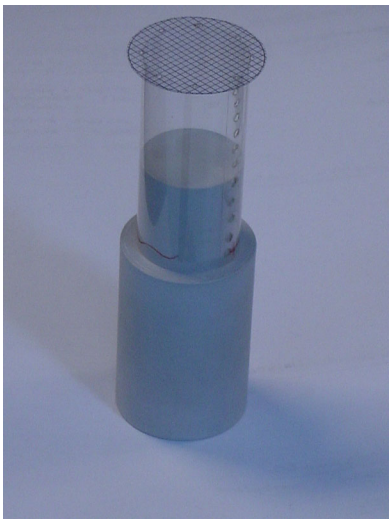

Fig 4. Photo of calibration grid on holder.

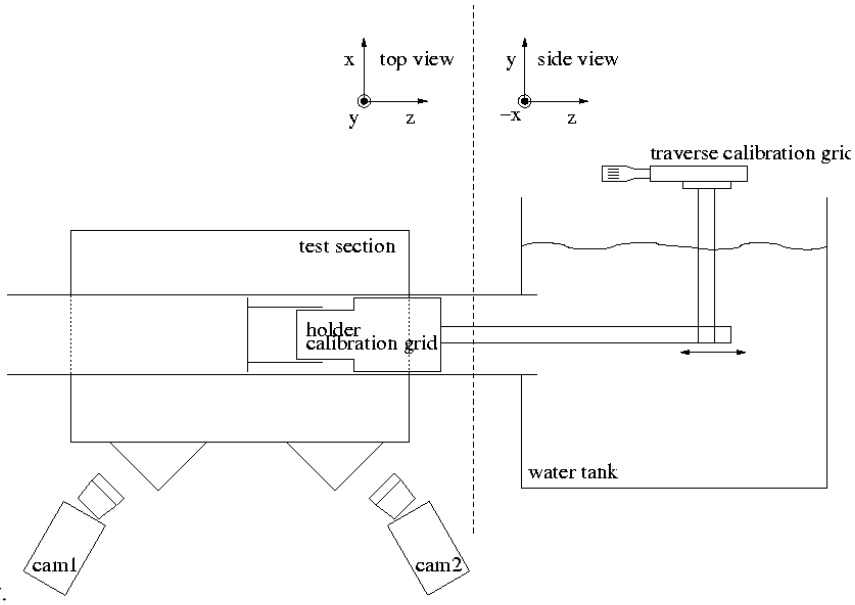

Fig 5. A water tank is placed after the test section to enter the calibration grid in the pipe and traverse it.

The data acquisition system is a commercial system from LaVision including the software (Davis 6.1.1.) used to evaluate the vector fields. The vector analysis was done for each camera in two steps. The first step used 64x64 non-preshifted interrogation windows, after which bad vectors were removed and replaced with help of a median filter. The second step uses the vector field of the first step for preshifting 32x32 interrogation areas. After this the vector fields of both cameras are combined (using the 3d calibration) and bad vectors were removed but not replaced from the 3D vector field.

3. Measurement uncertainty

For all kinds of stereo-PIV systems equations have been derived to calculate the 3D displacement vectors from the displacement data from the 2 cameras, see Prasad (2000). In al these equations the real dx, dy and dz displacements are linear functions of the displacements dx_1, dy_1, dx_2 and dy_2 seen by the two cameras. The proportionality constants depend on the geometry and exact location in the object plane (x, y) and can be expressed in several ways. A general form derived by Willert (1997) reads:

$$\begin{aligned} dx &= \frac{dx_2 \cdot \tan\alpha_1 - dx_1 \cdot \tan\alpha_2}{\tan\alpha_1 - \tan\alpha_2} \\ dy &= \frac{dy_1 - dy_2}{2} + \frac{dz}{2}(\tan\beta_2 - \tan\beta_1) \\ dz &= \frac{dx_2 - dx_1}{\tan\alpha_1 - \tan\alpha_2} \end{aligned} \qquad (1)$$

More elaborate error analysis takes into account, not only the interrogation errors in dx_1, dy_1, dx_2 and dy_2, but also the errors of all proportionality constants. In the case of a 2D calibration method this will include e.g. uncertainties in the nominal magnification factor and the distance between the lenses, see Prasad (2000). For a 3D calibration method the uncertainty in the proportionality constants is probably very small, because they are derived from the calibration. The exact uncertainty is very hard to estimate and will depend on both the calibration images and the mathematical methods used to derive the constants.

If we are only interested in an estimate of the order of magnitude of the errors, the error analysis becomes very simple. We assume that interrogation errors will dominate (in our 3D calibration system) and are all of the same order ($rms(dx_1)=rms(dy_1)=rms(dx_2)=rms(dy_2)=\sigma_{int}$). Then we substitute the characteristic angles of our geometry ($\alpha_1=45°,\ \alpha_2=135°,\ \beta_1=\beta_2=0°$) in eq.1 to obtain:

$$\begin{aligned} dx &\approx \frac{-dx_1 + dx_2}{\sqrt{2}} \\ dy &\approx \frac{dy_1 + dy_2}{2} \\ dz &\approx \frac{dx_1 + dx_2}{\sqrt{2}} \end{aligned} \Rightarrow \begin{aligned} \sigma_{dx} &\approx \sigma_{int} \\ \sigma_{dy} &\approx \frac{1}{2}\sqrt{2} \cdot \sigma_{int} \\ \sigma_{dz} &\approx \sigma_{int} \end{aligned} \qquad (2)$$

σ_{int} typically is of the order of 0.1 pixel (Westerweel *et al.* (1997)) which results in $\sigma_{dx}=\sigma_{dz}=0.1$ pixel and $\sigma_{dy}=0.07$ pixel.

Registration error

In the previous analysis it was assumed that the only error in dx_1, dy_1, dx_2 and dy_2 is due to the interrogation errors. There are, however, other contributions that are called registration errors. Although the notion registration error has been mentioned before by Prasad & Adrien (1973), Willert (1997) and Prasad (2000), it was not quantified. The following is not a thorough error analysis, but it will explain the background of the registration error and make clear it can not be neglected.

Registration error is due to the mismatch of the 2 dewarped (back projected) vector fields of camera 1 and 2. It causes velocity information from different regions of the illuminated field to get combined leading to errors in the 3D vector field. This would occur e.g. if the (dewarping) mapping function from the image plane to the physical plane is not accurate. This is not hypothetical for geometric reconstruction. For 2D or 3D calibrated systems, however, the mapping error is likely to be very small (around 1 pixel).

A second mechanism leading to registration errors is when the centre of the light sheet does not exactly coincide with the location of the calibration grid (i.e. the plane of back projection in physical space). Figure 6 shows this situation. In point (z_0,x_0) on the calibration plane a 3D vector (V_{piv}) is reconstructed from the two 2D displacement vectors v'_1 and v'_2 measured by camera 1 in (z_1,x_1) and by camera 2 in (z_2,x_2) on the measurement plane, i.e. the plane of the light sheet. To keep the explanation brief we will investigate the special case shown in the figure

($\alpha_1 = \alpha_2 = 45°$ and 2D shear flow), which corresponds to our set up. Writing $v_1=v_0+dv_1$ and$v_2=v_0+dv_2$ and drawing the vectors as in the left part of figure 6, it can be seen that
$v_{err} = dv_1 = dv_2 = \partial v_z/\partial x \cdot dx = \partial v_z/\partial x \cdot dz \equiv e(v_x)$, and in a similar way one obtains $e(v_z) = \partial v_x/\partial x \cdot dz$ where dz is the misalignment of the light sheet with respect to the calibration plane. Understanding this principle, it shouldn't be hard to derive expressions for a more general case.

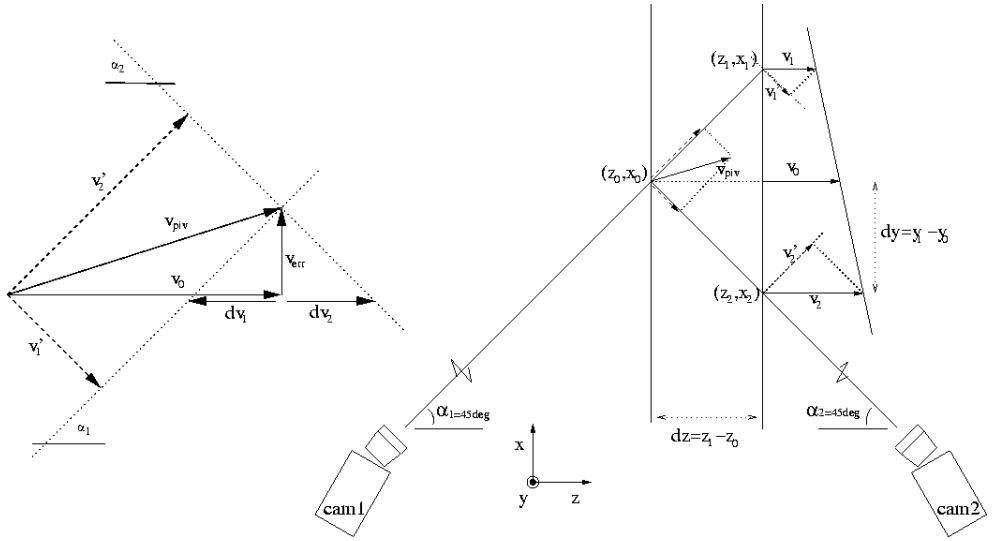

Fig 6. Drawing to explain the registration error in shear flow.

Measurement of the registration error

For laminar pipe flow we have a large velocity gradient close to the wall and the in-plane velocities v_x and v_y are zero. Making PIV recordings at different z-positions of the light sheet it is possible to measure $e(v_x)$ as function of dz. Figure 7 shows a vector field with considerable registration error in the v_x component.

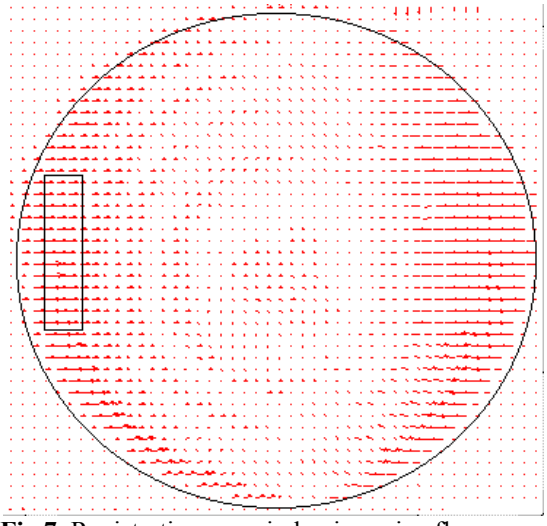

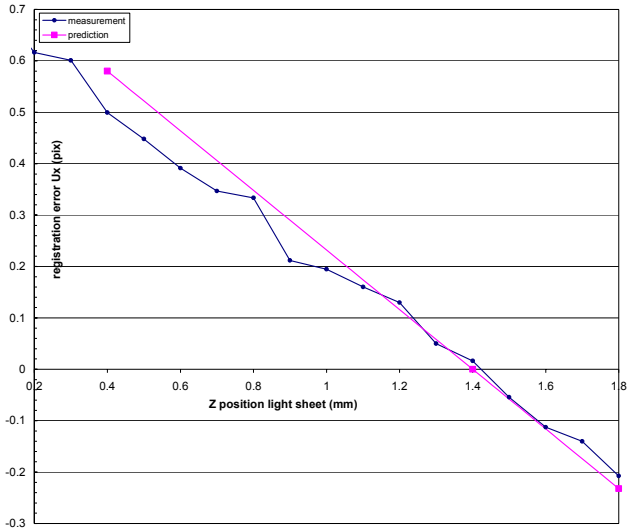

Fig 7. Registration error in laminar pipe flow.

Fig 8. Average registration error of the rectangle in fig. 7 as function of the position of the light sheet.

In the center of the pipe the velocity gradient is zero and no registration error occurs ($e(v_x)$ =0). The registration errors are different on both sides of the center because the grid is not completely flat and dz thus varies over space. The average of $e(v_x)$ as measured in the rectangle (close to the wall of the pipe) shown in figure 7 is plotted as function of the position of the light sheet (z) in figure 8.

To verify our conceptual understanding of the registation error, an estimate of the order of magnitude of $e(v_x)$ can be made. The parabolic profile and velocity gradients are : $v_z = v_c(1-(x/R)^2)$, where v_c is the centreline velocity and R is the radius of the pipe. The velocity gradient close to the wall is thus $\partial v_z/\partial x\,(R) = -2 \cdot v_c/R$. Now $e(v_x) = \partial v_z/\partial x\, dz = (-2 \cdot v_c/R) \cdot dz \rightarrow e(v_x)/v_c \approx 2 \cdot (z - z_0)/R$. This estimate is also plotted in figure 8 for v_c=5.8 pixels, R=20mm and z_0=1.4mm. The measured data are somewhat below the estimated line because they are taken in the rectangle at some distance from the wall**,** but on the whole the data follow our estimate very well.

We can conclude that if we want to measure v_x with a precision of 1% of the center line velocity (v_c), the misalignment dz can be at most 0.1mm. In turbulent flow the velocity gradients are even larger than in laminar flow and the required alignment precision becomes even stricter.

The calibration grid used so far is made of printed overhead sheet and therefore not completely flat. The deviation was estimated to be 0.3mm by looking with a camera under 45 degrees to the printed lines on the sheet. With this calibration sheet it is thus impossible to eliminate the registration error over the entire cross section of the pipe. In the future we will make use of a grid marked on a 0.5mm thick glass plate. One of the two cameras has to look through the thin glass plate, which will result in a small error in the mapping function. This error is however constant over the entire cross section and probably not too difficult to correct for.

Minimization of the registration error

The registration error depends on the flow gradients and is therefore in time dependent flow not a systematic error. The only way to overcome registration errors is to prevent a wrong combination of the dewarped vector fields of cameras 1 and 2. The solution is that after calibration the coincidence of the light sheet and calibration plane has to be checked. For this purpose one can use a known laminar shear flow, as we have shown in the previous section. However, in most experiments it might be impossible to create a well-known laminar flow for this purpose.

A second method to check the coincidence of the light sheet and calibration plane, as proposed by C. Willert (1997), is to take (particle) images of cameras 1 and 2 which have been recorded at the same time, map them into physical space and make a cross-correlation. The resulting displacement vectors are linearly proportional to the misalignment of the light sheet. This method works very well for a thin light sheet. For thick light sheets however, particles have in general different distances to the calibration plane, which result in different (imaginary) displacements when projected on the calibration plane. This leads to a wider and noisier correlation peak for the cross-correlation. If the light sheet becomes too thick, this method does not work at all. Translating a single lens of the light sheet optics is often enough to change the light sheet thickness. In principle, the alignment can thus be done with a thin light sheet using the cross correlation technique, after which the light sheet thickness can be increased if this is necessary for the experiments. One should however be aware that changing the light sheet thickness can also change the position of the center of the light sheet (as has happened to the authors) after which the alignment between the planes of the calibration and the light sheet is destroyed.

A third option to minimize registration errors would be to use the results of the cross correlation of camera 1 and 2 to correct the mapping functions from the image plane to the calibration plane. If one obtains a good cross correlation for the desired light sheet thickness, this might well be easier than adjusting the light sheet.

Laminar flow

After we have calibrated the PIV system and optimized the alignment of the light sheet and calibration plane, the first test has been to measure the parabolic velocity profile of Hagen-Poiseuille pipe flow. The streamwise velocity component is shown together with a parabolic fit in fig. 9. The measured profile is slightly asymmetric which is probably due to a small angle between the pipe in the test section and the upstream pipe sections. The maximal deviation is 0.25 pixel. Figure 10 shows the cross-flow (v_x, v_y) which is mainly due to registration error and takes a maximum value of 0.3 pixel. We have tried to remove the registration error with the alignment procedure of the light sheet but we did not succeed completely because of the 0.3mm non-flatness of the calibration grid.

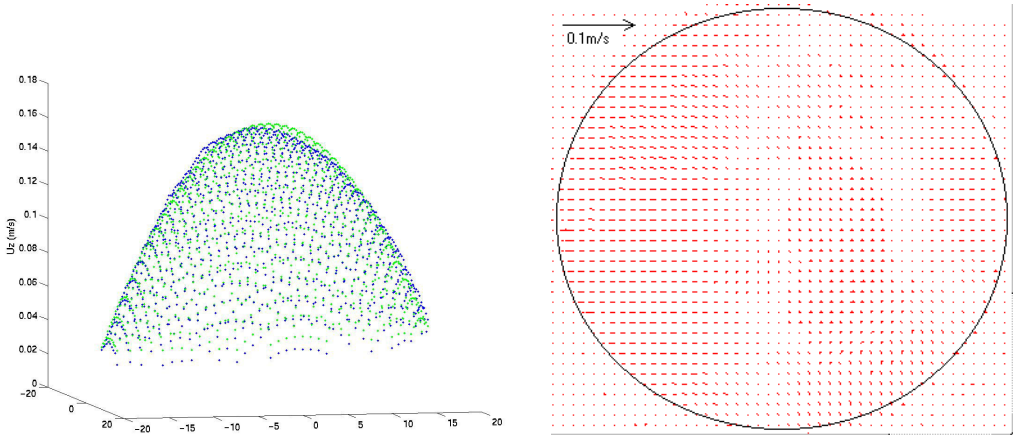

Fig 9. Measurement streamwise velocity laminar flow at Re=3000 and parabolic fit.
Fig 10. Measurement cross flow laminar flow (=registration error) at Re=3000.

Turbulent flow

A second test to validate our PIV system is to measure the turbulent statistics and compare the results with other data. At the moment we cannot interpret the results into meaningful statements about the precision of a single velocity estimate (1 vector) and this test shows rather the ability of the system to measure flow fluctuations.
In fig. 1 we show a single turbulent vector field at Re = 5300. Next we have used 380 turbulent vector fields taken at 15 Hz over a period of 25 seconds, which is about 80 integral time scales. The bulk velocity (U_b) has been determined by integrating the mean turbulent profile, which gives a somewhat low estimate, because the measured profiles fall off to quickly in the wall region. The friction velocity u*, used to normalize the data, was calculated from U_b and Blasius' law for the skin friction coefficient, see Westerweel *et al*. (1996). The result for u* has been estimated to be 9.35 (mm/s), which is somewhat too low due to the error in the bulk velocity Ub. The mean velocity profile obtained from this data set is shown in Fig. 11, the turbulent intensities in Fig. 12 and the Reynolds stress in Fig. 13. In these figures we also show the DNS data from Eggels *et al.*(1993. In the central region, the PIV system seems to measure the turbulence fluctuations quit reliably. The turbulent fluctuations are somewhat underestimated, which might be caused by the spatial averaging over the interrogation areas of the PIV technique. Close to the wall, large deviations occur and data in this region is influenced by large errors.

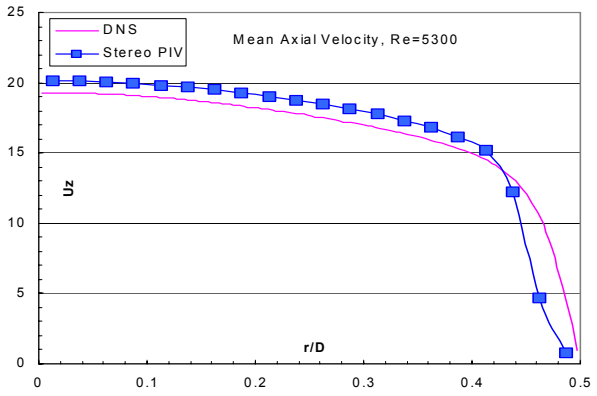

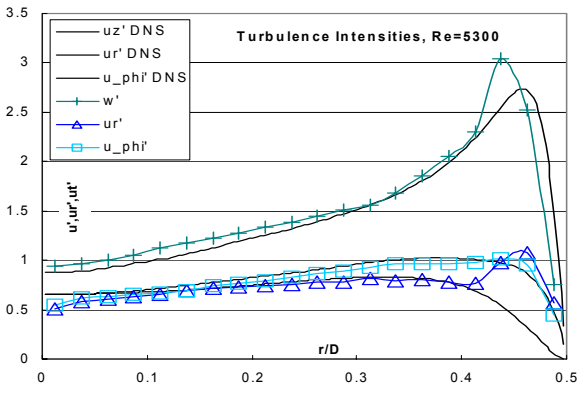

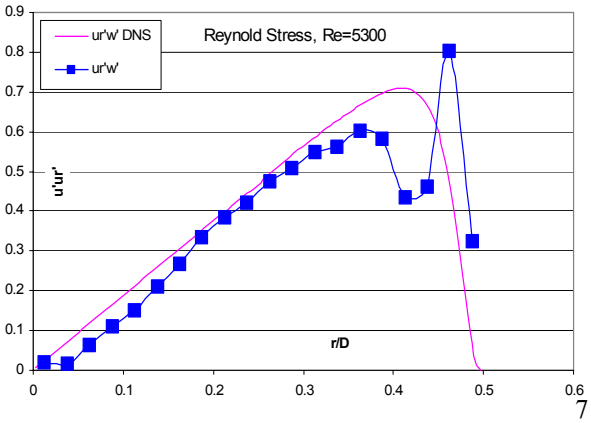

Fig. 11. Mean turbulent profile of axial velocity
Fig. 12. Mean profile of turbulent fluctuations axial, radial and tangential velocity component
Fig. 13. Mean Reynolds stress profile.

4. Transition measurements

The data presented in this paragraph is the result of some very brief test runs and can best be seen as a test of the measurement concept and **as** an example of the kind of experiment we will conduct in the near future.

Disturbance mechanism

We have designed a disturbance mechanism which is able to match perturbations used in the DNS simulations of Ma *et al.*(1999) where time-periodic blowing and suction is applied over the full circumference of the pipe and over a distance of one pipe diameter in the streamwise direction. To mimic this boundary condition in our experiment, we have at some position replaced the pipe wall by a tube of porous metal. The pore size of the porous metal is so small (40 mu) that the injected flow is laminar and homogeneous over the whole extent of the porous wall. Two chambers are built around the porous tube, when fluid is injected from one side suction is applied on the opposite side. The blowing and suction is forced by two syringes, which are moved by a computer controlled servo motor. Figure 14 shows two instantaneous flow fields at about 3 pipe diameters downstream of a large fluid injection through the porous wall. In this case the fluid injection was done manually.

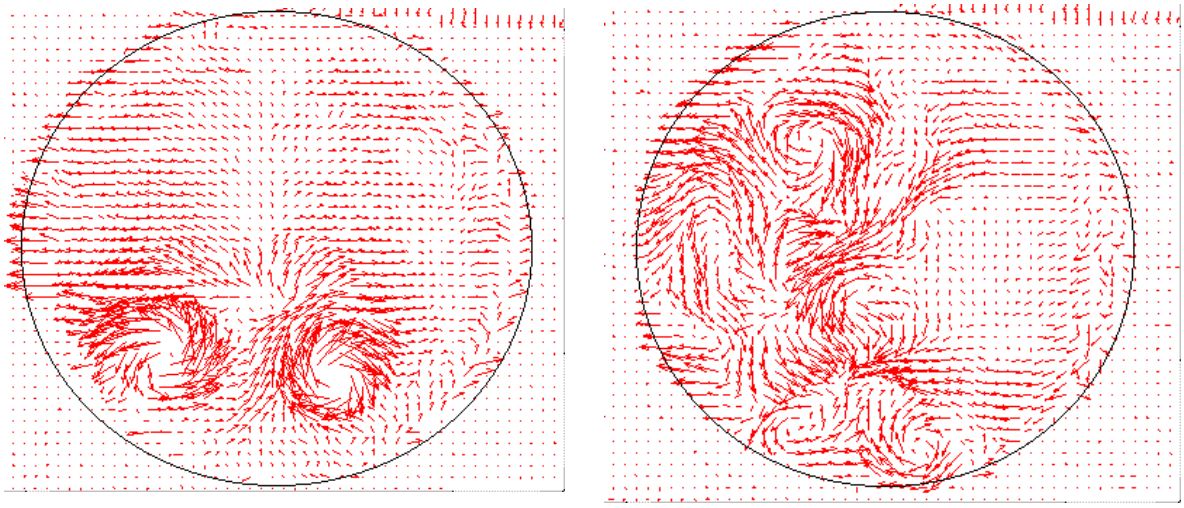

Fig 14. Two different flow fields downstream of a fluid injection trough the porous wall.

Puff

A puff is for a pipe flow the equivalent of turbulent spot in a boundary layer. Puffs and slugs have been studied by Wygnanski & Champagne (1973), Wygnanski *et al.* (1975) and Darbyshire & Mullin (1995). We have created a puff by manually injecting some dye-colored fluid trough a hole about 100 pipe diameters upstream from the measurement section. By following the dye, the PIV recording we have started manually when the flow disturbance passed the test section. A series of 190 measurements at 15 Hz have been recorded. Figure 15 shows the centerline velocity of 2 series, which correspond to passing of the leading and trailing edge of a puff. Figure 16 shows the cross flow at the 4 positions indicated in figure 15. The mean laminar flow field has been subtracted from the vector fields to accentuate the flow patterns. From the smooth behavior of the centerline velocity it looks like the 15 Hz sample rate is high enough to resolve the temporal evolution and make a movie of the subsequent vector fields.

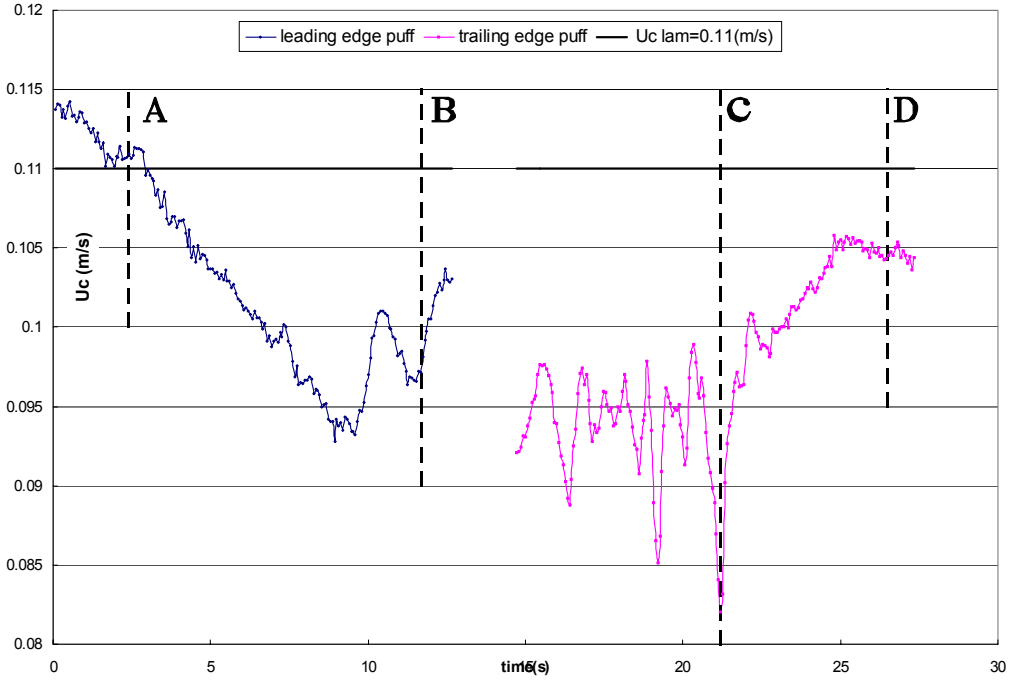

Fig 15. Centerline velocity in the leading edge and trailing edge of a puff at Re=2000.

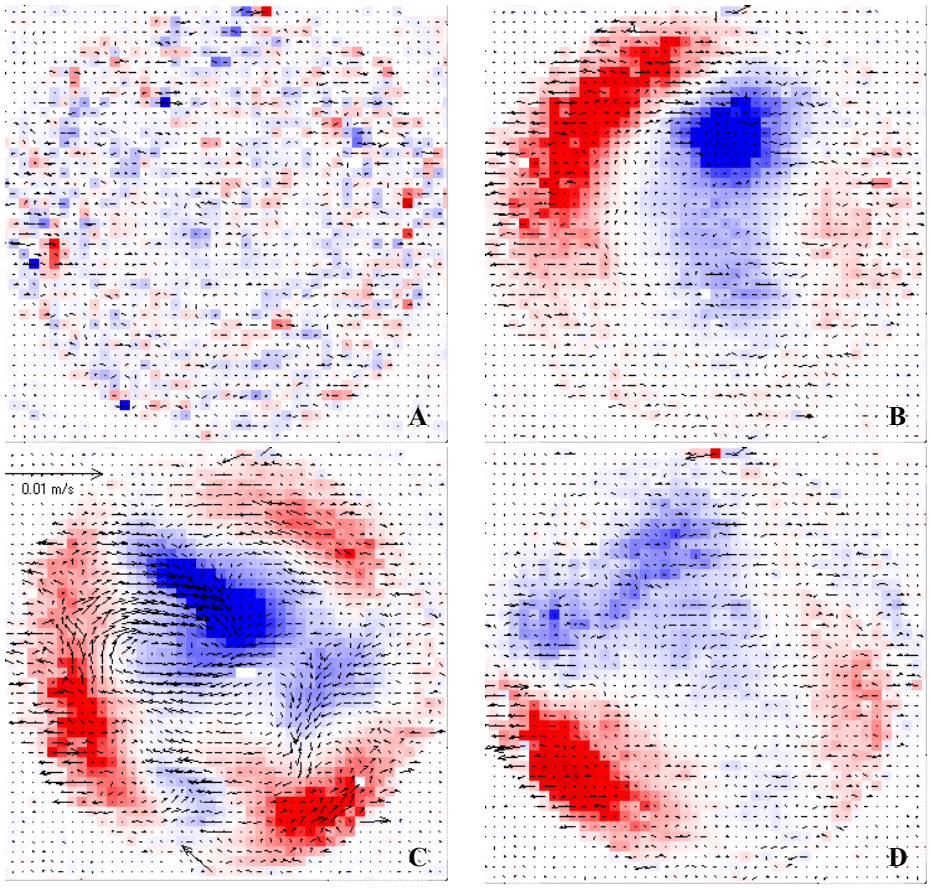

Fig 16. Cross flow measurements in a puff, A,B,C and D are also indicated in fig. 15. The laminar profile has been subtracted and the color represents the z-component of the 3D vector field (red is positive, blue is negative).

5. Conclusions and outlook

The conclusions have already been summarized in the abstract at the beginning of this paper. Therefore we restrict ourselves here to giving an outlook.

To minimize the registration error in the future, we intend to use a 0.5mm thick glass calibration grid. Further improvements of the PIV measurements may consist of changing the resolution to 16x16 interrogation areas.

Transition measurements of laminar pipe flow disturbed by periodic blowing and suction from the wall will be carried out. By combining measurements that are phase locked to the disturbance and from several downstream locations a 3D reconstruction of the transition can be obtained. Also the strength and location of stream-wise vortices will be measured.

The injection mechanism can also be used to make a short strong flow perturbation that will develop into a puff. Adjusting the delay between the puff generation and the PIV recordings, detailed study can be made of the leading and trailing edge where respectively relaminarisation and transition occur.

References

Darbyshire, A.G., Mullin, T. (1995). Transition to turbulence in constant-mass-flux pipe flow, *J. Fluid Mech.*, **Vol. 289**, pp. 83-114.

Draad, A.A., (1996) Laminar-turbulent transition in pipe flow for Newtonian and non-Newtonian fluids, *Ph.D. Thesis, Delft University of Technology*.

Draad, A.A., Kuiken, G.D.C., Nieuwstadt, F.T.M., (1998) Laminar-turbulent transition in pipe flow for Newtonian and non-Newtonian fluids, *J. Fluid Mech.*, **Vol. 377**, pp.267--312.

Eggels, J.G.M., Westerweel, J., Nieuwstadt, F.T.M. (1993). Direct numerical simulation of turbulent pipe flow. *Appl. Sci. Res.* **Vol. 51**, pp.319-324.

Eliahou, S., Tumin, A., Wygnanski, I. (1998) Laminar-turbulent transition in Poiseuille pipe flow subjected to periodic perturbations emanating from the wall, *J. Fluid Mech.,* **Vol. 361**, pp 333-349.

Ma, B., Doorne, C.W.H., Zhang, Z., Nieuwstadt, F.T.M. (1999). On the spacial evolution of a wall-imposed periodic disturbance in pipe Poiseuille flow at *Re* = 3000. Part1. Subcritical disturbance, *J. Fluid Mech.,* **Vol. 398**, pp. 181-224.

Prasad, A.K., Adrian, R.J. (1993), Stereoscopic particle image velocimetry applied to liquid flows, *Exp. Fluids,* **Vol. 15**, pp. 49-60.

Prasad, A.K. (2000), Stereoscopic particle image velocimetry, *Exp. Fluids,* **Vol. 29**, pp 103-116.

Reynolds, O.(1883). An experimental investigation of the circumstances which determine whether the motion of water shall be direct of sinuous, and the law of resistance in parallel channels, *Phil. Tran. R. Lond.* **Vol. 174**, pp. 935-982.

Soloff, S.M., Adrian, R.J., Liu, Z.C. (1997). Distortion compensation for generalized stereoscopic particle image velocimetry. *Meas. Sci. Technol.,* **Vol. 8**, pp. 1441-1454.

Westerweel, J., Dabiri, D., Gharib, M., (1997). The effect of a discrete window offset on the accuracy of cross-correlation analysis of digital PIV recordings, *Exp Fluids,* **Vol. 23**, pp 20-28.

Westerweel, J., Draad, A.A. (1996) Measurement of temporal and spatial evolution of transitional pipe flow with PIV, *Development in laser techniques and fluid mechanics, 8th International Symposium, Lisbon, Portugal, 8-11 Luly, 1996,* pp. 311-324.

Westerweel, J., Draad, A.A., van der Hoeven, J.G.Th., van Oord, J. (1996). Measurement of fully-developed turbulent pipe flow with digital particle image velocimetry, *Exp.Fluids,* **Vol 20**, pp. 165-177.

Willert, C. (1997). Stereoscopic digital particle image velocimetry for application in wind tunnel flows. *Meas. Sci. Technol.,* **Vol. 8**, pp1465-1479.

Wygnanski, I.J., Champagne, F.H. (1973). On transition in a pipe. Part 1. The origin of puffs and slugs and the flow in a turbulent slug. *J Fluid Mech,* **Vol. 59**, pp. 281-335.

Wygnanski, I., Sokolov, M., Friedman, D. (1975). On transition in a pipe. Part 2. The equilibrium puff. *J Fluid Mech.,* **Vol. 69**, pp. 283-304.